Ginzburg-Landau parameter in $YBa_2Cu_3O_{6.95}$ below the irreversibility temperature as measured by μ^+SR in high magnetic fields

T.M. Riseman,* J.H. Brewer. K.H. Chow,† W.N. Hardy, R.F. Kiefl, S.R. Kreitzman, R. Liang, W.A. MacFarlane, P. Mendels,‡ G.D. Morris, J. Rammer,§ and J.W. Schneider**
TRIUMF, Canadian Institute for Advanced Research and Department of Physics, University of British Columbia, Vancouver, British Columbia, Canada V6T 1Z1

C. Niedermayer
Fakultät für Physik, Universität Konstanz, D-7750 Konstanz, Germany

S.L. Lee
Physik-Institut der Universität Zürich, CH-8057 Zürich, Switzerland
(Received 7 February 1995)

The vortex state of a type-II superconductor produces a distinctive μ^+SR line shape with features determined by the average internal field B_0, the magnetic penetration depth λ, the superconducting coherence length ξ, and the degree of disorder in the vortex lattice. Only in the high field regime ($\lambda \gg L > \xi$, where L is the intervortex spacing) do the vortex cores (of radius $\approx \xi$) occupy a large enough area that they are observable in the line shape as a high field cutoff. Our μ^+SR measurements of the field distributions in a mosaic of single crystals of $YBa_2Cu_3O_{6.95}$ in fields of 1.9, 4.1, 4.7, and 6.5 T ($\mathbf{B}_0 \parallel \hat{\mathbf{c}}$) show all the features of the line shape. We find $\lambda = 0.15 \pm 0.01$ μm at 10 K and the Ginzburg-Landau parameter $\kappa \equiv \lambda/\xi = 69.6 \pm 1.4$ constant between 30 and 75 K; this is the only measurement to date of κ in $YBa_2Cu_3O_{6.95}$ below the irreversibility temperature. Due to disorder in the vortex lattice, either from pinning or from vortex fluctuations that are quasistatic on the time scale of μ^+SR, the observed line shape is "smeared" relative to that predicted for a perfect lattice. From the degree of smearing, we estimate an upper limit of 5.5% for the rms deviation of individual vortices from their ideal positions.

I. INTRODUCTION

This paper presents a determination of the magnetic penetration depth λ and the superconducting coherence length ξ in the optimally oxygenated high-temperature superconductor $YBa_2Cu_3O_{6.95}$, based upon positive muon spin rotation (μ^+SR) measurements of the local field distribution $n(B)$ in single-crystal mosaic samples. Magnetic fields $\mathbf{B}_0$ of 1.9 T, 4.1 T, 4.7 T, and 6.5 T were applied parallel to the crystalline $\hat{\mathbf{c}}$ axis for temperatures between 10 K and 75 K. Since all the results reported here are for $\mathbf{B}_0 \parallel \hat{\mathbf{c}}$, an isotropic London treatment is appropriate: λ refers to the magnetic penetration depth in the copper oxide planes (λ_{ab}), $\mathbf{H}_{c2}$ refers to $\mathbf{H}_{c2} \parallel \hat{\mathbf{c}}$, and so on. Any possible effects of in-plane ($\hat{\mathbf{a}}$-$\hat{\mathbf{b}}$) anisotropy have been neglected.

An extensive analysis is performed using a modified London model, which employs a cutoff in the reciprocal lattice vectors to make the field finite at the vortex core and introduces a term $(1 - B_0/H_{c2})$ to take into account the field dependence of the superconducting order parameter. When the average internal field B_0 is below about 25% of the upper critical field H_{c2} and the Ginzburg-Landau parameter $\kappa = \lambda/\xi$ is large, the line shape produced by this model closely matches the features of the exact theoretical line shape produced from Gorkov's s-wave-based equations[1–3] while being relatively easy to express mathematically. In order to calculate the field distribution $n(B)$ using the Gorkov treatment, one must make assumptions about the Fermi surface and the degree of strong coupling which are tantamount to assuming the form of $\lambda(T)/\lambda(0)$ and $\xi(T)/\xi(0)$ — the very temperature dependences one wishes to measure experimentally. Faulty assumptions may lead, for instance, to false temperature dependences for κ. On the other hand, the modified London model (being phenomenological and involving as parameters only the average internal field B_0, the magnetic penetration depth λ, and the superconducting coherence length $\xi \propto H_{c2}^{-\frac{1}{2}}$ at a given temperature) requires no such assumptions in calculating $n(B)$. The effects of the Fermi surface, strong coupling, s- or d-wave pairing, and so on may be inferred from the temperature dependence found for λ and ξ. Moreover, the modified London model is much faster to calculate.

The distribution $n(B)$ is very asymmetric (see Fig. 1), with a cusp below the average field and a long high field tail corresponding to the high fields near the vortex cores in the vortex or flux line lattice (FLL). Its overall linewidth is predominantly proportional to λ^{-2}. The coherence length serves primarily to introduce a high

field cutoff at the field just outside the vortex core; however, at fields which are non-negligible compared with H_{c2}, this cutoff effectively narrows $n(B)$ so that the linewidth depends upon ξ as well as λ. Because the distribution $n(B)$ is more sensitive to λ than to ξ, the former could be much more accurately determined if one could fix ξ (or, equivalently, H_{c2}) from other experiments. However, the tremendously high value of $H_{c2}\,|_{T\to 0}$ in $YBa_2Cu_3O_{7-\delta}$ makes it quite difficult to measure directly, as reflected in the inconsistency between values of $H_{c2}\,|_{T\to 0}$ ($\mathbf{B}_0 \parallel \hat{\mathbf{c}}$) reported in the literature, which vary from 40 T (from pulsed fields[4]) to 130 T (from de Haas–van Alphen oscillations using explosively driven pulsed magnets[5]) to 140 T (from resistivity using explosively driven pulsed magnets[6]). Lower bounds for $dH_{c2}/dT\,|_{T_c}$ can be determined from ac and dc resistivity measurements using conventional static magnets, but measurements of H_{c2} near T_c are complicated by fluctuation effects as well as flux flow, flux creep, and glassy vortex phase transitions. Perhaps the most reliable estimates of $dH_{c2}/dT\,|_{T_c}$ have been made using magnetization measurements in the reversible regime near T_c, giving values ranging from -1.65 T/K in a single $YBa_2Cu_3O_7$ crystal[7] to -1.90 T/K in an aligned $YBa_2Cu_3O_{7-\delta}$ powder suspended in epoxy.[8] However, extrapolating $H_{c2}(T)$ over the whole temperature range from values close to T_c is risky at best, since it once again requires assumptions about the temperature dependence of H_{c2}, which is affected by the degree of strong coupling, a three-dimensional (3D) or 2D Fermi surface, etc.

Since a consensus on $H_{c2}(T)$ well below T_c is certainly lacking, we cannot assume a T dependence of ξ in our analysis of μ^+SR frequency spectra. Fortunately, by simultaneously fitting $n(B)$ data from several μ^+SR runs at the same temperature and different fields, we have been able to independently determine both λ *and* ξ at each temperature.

II. DETERMINATION OF THE FIELD DISTRIBUTION USING THE μ^+SR TECHNIQUE

The positive muon (μ^+) is a spin 1/2 lepton (with a mass approximately one-ninth of a proton) which, as a decay product of a positive pion at rest, is spin polarized antiparallel to its momentum. In a transverse field muon spin rotation (TF-μ^+SR) experiment, muons are implanted one at a time in the bulk of a sample to which a magnetic field is applied perpendicular to the muon polarization. Just before implantation, the incoming muon passes through a thin scintillator, called the muon counter, which starts a LeCroy 4204 TDC (the "clock"). Once stopped in the sample at a random location $\mathbf{r}$, the muon precesses about the local magnetic field $\mathbf{B}$ ($\mathbf{r}$) at the Larmor frequency $\omega = \gamma_\mu B(\mathbf{r})$, where $\gamma_\mu = 2\pi \times 135.5$ MHz/T. With a mean lifetime $\tau_\mu = 2.197\,\mu$s, the muon decays into a positron, a neutrino, and an antineutrino. The high-energy (up to 52.8 MeV) positron is preferentially emitted along the muon spin direction (due to parity symmetry violation in the weak interaction) and is detected by one or more thick scintillation counters; the resultant e^+ trigger stops the clock. The time dependence of the muon ensemble polarization is recorded by histogramming many such time intervals between each muon entering the sample and its decay in a given direction. Several such histograms are accumulated, one for each positron detector, which defines a decay direction and therefore a muon polarization component. For the case of two positron counters (indicated below by + and −) on opposite sides of the sample, defining an axis perpendicular to the applied field, the number of events in the μSR histograms may be written as

$$N_\pm(t) = N_0^\pm\,[1 \pm A_\pm P(t)]\,e^{-t/\tau_\mu} + B_\pm, \tag{2.1}$$

where $N_0^\pm$ are normalization constants, $A_\pm$ are the empirical maximum positron decay asymmetries (corresponding to full muon polarization along that axis), $P(t)$ is the time evolution of the muon polarization along said axis, and $B_\pm$ are time-independent random backgrounds.

When the transverse components of the local field are very small compared to the magnitude B_o of the average internal field ($|\mathbf{B}(\mathbf{r}) - \mathbf{B}_0| \ll B_0$), as was the case in the experiment discussed in this paper, the relationship between the muon polarization function and the internal fields is particularly simple:

$$P(t) = \frac{1}{V}\int_V \cos\left[\gamma_\mu B(\mathbf{r})t + 2\pi\theta\right]\,d^3r, \tag{2.2}$$

where V is the volume of the sample and the angle θ is the initial angle of the muon spin relative to the + counter. This equation can be rewritten as a Fourier transform,

$$P(t) = \int n(B)\cos\left[\gamma_\mu B t + 2\pi\theta\right]\,dB, \tag{2.3}$$

where the weighting factor $n(B)$, called the Fourier transform's *line shape*, represents the fraction of the sample which has a particular local field magnitude B (within dB). This line shape may thus be extracted from the experimental polarization function $P(t)$ using standard Fourier transform techniques.[9]

III. VORTEX LATTICE AND THE MODIFIED LONDON MODEL

In an isotropic superconductor, the vortices preferentially form a triangular lattice[10,11] at positions

$$\mathbf{r}_v = n_1\,(L\hat{\mathbf{x}}) + n_2\left(L\frac{1}{2}\hat{\mathbf{x}} + L\frac{\sqrt{3}}{2}\hat{\mathbf{y}}\right), \tag{3.1}$$

where n_1 and n_2 are integers and

$$L = \left(\frac{2\phi_0}{\sqrt{3}B_0}\right)^{\frac{1}{2}} \tag{3.2}$$

is the intervortex spacing; $\phi_0 = 2.068\times 10^{-15}$ T m^2 is the

flux quantum and B_0 is the average internal field. The isotropic London model, which ignores the vortex cores (i.e., assumes $\xi \ll L$ as well as $\xi \ll \lambda$), predicts that the local fields are given by

$$B(\mathbf{r}) = B_0 \sum_{\mathbf{k}} \frac{\exp[-i\mathbf{k}\cdot\mathbf{r}]}{1+k^2\lambda^2}, \tag{3.3}$$

where $\mathbf{k}$ are the reciprocal lattice vectors of $\mathbf{r}_v$. When the London model is in the "medium field" limit, which is the case when B_0 is greater than the lower critical field H_{c1} (or $\lambda > L$), the extent of variations in $B(\mathbf{r})$, and consequently the linewidth of $n(B)$, is proportional to λ^{-2} (Fig. 1). When a field is applied along the symmetry axis of a uniaxial superconductor, the isotropic model is appropriate. In the case of $YBa_2Cu_3O_{7-\delta}$, which has only a modest anisotropy in the $\hat{\mathbf{a}}$-$\hat{\mathbf{b}}$ plane, the isotropic model will work well with an effective penetration depth ($\lambda_{\text{eff}} = \sqrt{\lambda_a \lambda_b}$) when $\lambda_{\text{eff}} > L$.

The field variation $B(\mathbf{r})$ within the triangular vortex lattice in a type-II superconductor produces a distinctive asymmetric line shape $n(B)$ in the Fourier transform (see Fig. 1). The point between three vortices, where the field has its minimum value, shows up as a shoulder-shaped cutoff at the left edge of the line shape. The saddle point between two vortices produces a Van Hove singularity which shows up as a cusp in the line shape well below the average field B_0. Since the field increases rapidly towards the center of a vortex, the distribution has a long high-frequency tail, which must actually have a cutoff at the maximum field located at the vortex core. Due to a finite critical current, the vortex core, defined by the absence of superconductivity, has a radius of approximately ξ, the coherence length of the supercurrent's carrier pairs.

In fields that are high enough that the vortex core size is no longer negligible, but are still smaller than approximately one-quarter of the upper critical field H_{c2}, the field distribution in an isotropic superconductor can be phenomenologically approximated by modifying the London model as follows:[2,3,12,13,1]

$$B(\mathbf{r}) = B_0 \sum_{\mathbf{k}} \frac{e^{-i\mathbf{k}\cdot\mathbf{r}} \exp\left[-\dfrac{\xi^2 k^2}{2(1-b)}\right]}{1+\dfrac{k^2\lambda^2}{1-b}}, \tag{3.4}$$

where $b = B_0/H_{c2}(T)$ is the reduced magnetic field. The exponential involving the coherence length ξ serves as a cutoff for the reciprocal lattice vectors at $k \approx 2\pi/\xi$, which yields a finite value for the magnetic field at the vortex cores. By contrast, the ordinary London model [Eq. (3.3)] predicts an infinite field at the center of the vortices. The term $(1-b)$ reflects the field dependence of the superconducting order parameter,[3,13] which, for constant B_0 and λ, causes a reduction in the overall width of the line shape with decreasing H_{c2} (see Ref. 14). The modified London model must be used rather than the regular London model at higher fields ($B_0 \gtrsim 0.05 H_{c2}$), because the area occupied by the vortex core becomes significant relative to the unit cell of the FLL. The maximum field in the vortex core produces a non-negligible

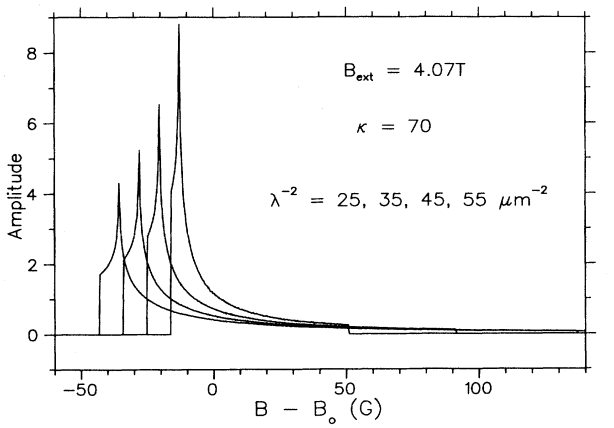

FIG. 1. Line shape as calculated by the modified London model [Eq. (3.4)] for an isotropic superconductor with $B_0 = 4.07\,\text{T}$, $\lambda^{-2} = 25.0$, 35, 45, and 55 μm^{-2} (narrowest to widest), and $\kappa = 70$.

cutoff amplitude in the μSR line shape $n(B)$ (Fig. 2). Moreover, the linewidth decreases both for increasing field (Fig. 2) and smaller κ (Fig. 3). If the weak-coupling BCS functions for $\xi(T)$ and $\lambda(T)$ are substituted into Eq. (3.4), the resulting line shapes closely match the line shapes obtained from Gorkov's s-wave-based equations.[1]

In isotropic BCS theory in the Ginzburg-Landau limit, the coherence length can be related to the upper critical field[15] by

$$H_{c2} = \frac{\phi_0}{2\pi\xi^2}. \tag{3.5}$$

Using this relation and recognizing that the reciprocal lattice vectors $\mathbf{k}$ are inversely proportional to the intervortex spacing L, Eq. (3.4) can be expressed as a function of only B_0, λ, and ξ or, alternatively, of B_0, λ^{-2}, and H_{c2} or B_0, λ^{-2}, and κ. In reality, the field distribution $B(\mathbf{r})$ is most directly determined by the coherence length rather than the upper critical field, because the exponential in-

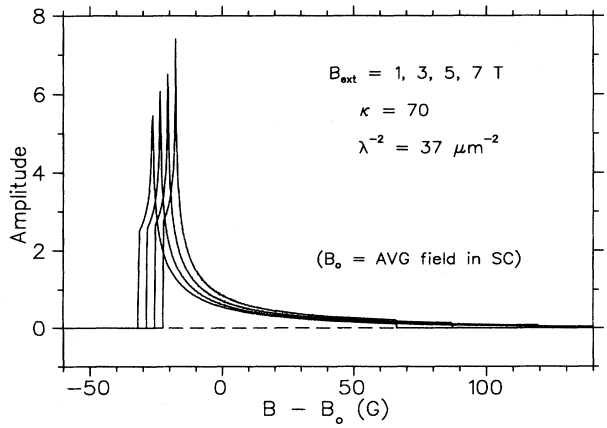

FIG. 2. Line shape as calculated by the modified London model [Eq. (3.4)] for an isotropic superconductor with $B_0 = 1$, 3, 5, and 7 T (widest to narrowest), $\lambda^{-2} = 37.0\,\mu\text{m}^{-2}$, and $\kappa = 70$.

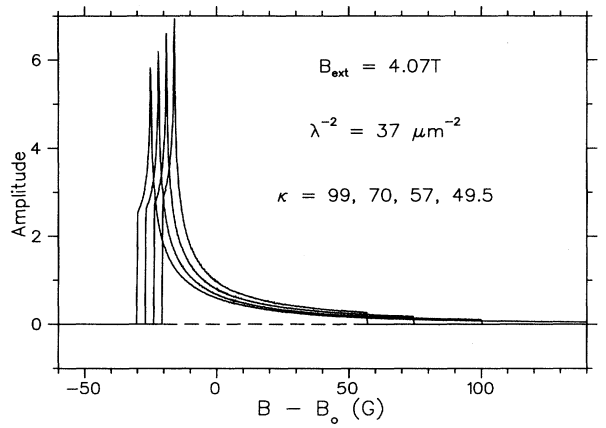

FIG. 3. Line shape as calculated by the modified London model [Eq. (3.4)] for an isotropic superconductor with $B_0 = 4.07\,\mathrm{T}$, $\lambda^{-2} = 37.0\,\mu\mathrm{m}^{-2}$, and $\kappa = 49.497\,48$, 57.153 77, 70.0, and 98.994 96 (narrowest to widest). These values of κ correspond to $\kappa^{-2} = 2.0 \times 70^{-2}$, 1.5×70^{-2}, 70^{-2}, and 0.5×70^{-2}.

volving the size of the vortex core ξ clearly uses a physical distance and the expression $(1 - b) < 1$ reflects the spatial portion of the sample where the order parameter is suppressed in and near the vortex cores. Therefore, if Eq. (3.5) does not hold exactly for all temperatures, as may be the case for theories other than weak-coupling BCS,[25] then it is more appropriate to express the reduced field as

$$b = \frac{4\pi}{\sqrt{3}} \left(\frac{\xi}{L}\right)^2, \tag{3.6}$$

rather than as $b = B_0/H_{c2}(T)$. Results for the Ginzburg-Landau parameter $\kappa = \lambda/\xi$ from analysis of μSR line shapes should be model independent regardless of whether $H_{c2}(T)$ is exactly proportional to $\xi^{-2}(T)$.

IV. DISORDER IN THE FLUX LINE LATTICE

If the FLL deviates from its ideal configuration as a perfect triangular array (due to dislocations, microscopic disorder, variations in the macroscopic average field, etc.), the theoretical μSR line shape will lose its sharp features at the minimum, cusp, and maximum fields. This means that the line shape of the experimental data cannot be adequately fitted to the theoretical line shape $n(B)$ for the ideal FLL alone. The theoretical line shape may be convoluted with a Gaussian distribution of fields,

$$n_s(B) = \int \frac{1}{\sqrt{2\pi}\sigma_B} \exp\left[-\frac{1}{2}\left(\frac{B - B'}{\sigma_B}\right)^2\right] n(B')\,dB', \tag{4.1}$$

a method successfully used in the analysis of μ^+SR data on Nb.[16] Brandt[2] showed that this convolution is consistent with how, in a stiff FLL, random disorder and distortions due to flux pinning modify the line shape from the ideal case.

The degree of the disorder can be estimated from the experimentally determined values of σ_B and λ. The vortex displacement is given by

$$\mathbf{s}_v(z) = \mathbf{r}_v(z) - \mathbf{r}_v^0, \tag{4.2}$$

where $\mathbf{r}_v^0$ is the location of the vth flux line in the ideal FLL. By assuming that the vortices are stiff and noting that the integrals of the exponentials are Dirac δ functions, using Eq. (43) in Ref. 2 we can estimate from σ_B the rms displacements $\langle s^2\rangle^{1/2}$ of the vortices from their ideal positions in the perfect FLL:

$$\langle s^2\rangle^{1/2} \approx \frac{\sigma_B}{B_0}\sqrt{2}\left(\sum_{\mathbf{k}\in\mathbf{k}_{BZ}} \frac{k_x^2 + k_y^2}{[1 + \lambda^2 k^2/(1-b)]^2}\right)^{-\frac{1}{2}}. \tag{4.3}$$

The summation is limited to the vortex lattice's first Brillouin zone (BZ), for which $0 \le k < 2\pi/L$, where L is the intervortex spacing. With small random distortions, the contribution to σ_B from random shear[2] is much smaller (by a factor of $\sim 10^{-3}$ in this experiment) than that from random compression[2] and is therefore neglected.

Figure 4 shows the amount of smearing corresponding to random disorder $\langle s^2\rangle^{1/2}/L$ of 0%, 2%, 4%, and 6%. Note that the cusp shifts higher towards the average field B_0 as the amount of disorder increases. This means that the average field as determined by a simple Gaussian fit of the line shape represents neither the average field nor the cusp field, which makes interpretation difficult.

It is important to remember that μ^+SR is only sensitive to variations in the magnitude of the local field, such as that caused by nearest-neighbor disorder in the FLL. Therefore, with μ^+SR one cannot distinguish between local deviations of vortices from their ideal positions in a FLL which retains its long-range hexagonal order and disorder which includes slow rotations or undulations of the FLL's unit vectors.[2]

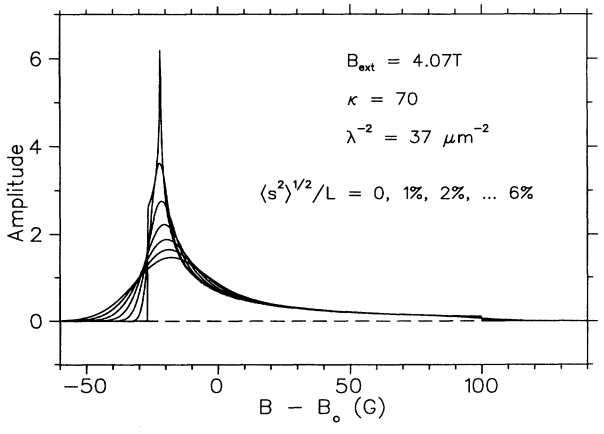

FIG. 4. Line shape as calculated by the modified London model [Eq. (3.4)] for an isotropic superconductor with $B_0 = 4.07\,\mathrm{T}$, $\lambda^{-2} = 37.0\,\mu\mathrm{m}^{-2}$, $\kappa = 70$, and $\langle s^2\rangle^{1/2}/L = 0\%$, 2%, 4%, and 6% (increasing broadening).

V. EXPERIMENT

A flux method was used to make high quality $YBa_2Cu_3O_{6.95}$ crystals, which were grown in yttria-stabilized zirconia crucibles and carefully oxygen annealed.[17] The width of their critical temperature transition was less than 0.25 K, with an onset at 93.5 K. Nineteen flat crystals with a typical thickness of 0.2 mm, ranging in area from 7.4 mm^2 to 0.26 mm^2 each, were mounted as a mosaic on an 8 mm diameter, 99.999% pure silver disk using Apiezon N grease, with the $\hat{\mathbf{c}}$ axis normal to the plane of the disk. The mosaic was closely fitted so that essentially none of the silver backing showed through. The sample was mounted in a liquid-helium-cooled cold finger cryostat inside the warm bore of the TRIUMF μSR User Facility's 7 T superconducting Helios magnet, mounted at the end of TRIUMF's M15 beam line. A carbon glass resistor thermometer was attached approximately 1 cm behind the sample. Magnetic fields between 1.9 T and 6.5 T were applied parallel to both the $\hat{\mathbf{c}}$ axis and the muon beam momentum. The muon spin was rotated perpendicular to the momentum before implantation by the use of crossed electric and magnetic fields.[18]

The μSR spectrometer used in this experiment consisted of one muon counter and two positron counters, all with parabolic surfaces designed such that, for a given counter, each light ray has roughly the same transit time; this geometry provides a better timing resolution than traditional paddle-shaped counters. The scintillators, placed at the foci of the parabolic reflecting surfaces, are of Pilot U plastic. When combined with a 7 T warm bore superconducting magnet, this high field, high timing resolution spectrometer made possible the highest transverse field μSR measurements reported to date. Figure 5 shows the portion of the apparatus (counters, cryostat, and beam pipe) which lies within the bore of the magnet.

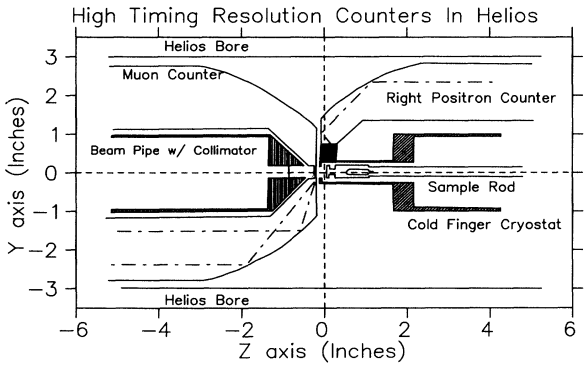

FIG. 5. High timing resolution apparatus. Several light paths are indicated by the dot-dashed lines. The crosshatched area is the scintillator for the right positron counter. The source of light rays for the muon counter is a 1 cm diameter by 500 μm thick scintillator. The roughly capsule-shaped groove near the end of the sample rod is the location of a carbon glass thermometer. Helios is a 7 T superconducting magnet with a 6-in. warm bore.

Outside the bore, additional parabolic surfaces refocus the light on mesh dynode photomultipliers, which tolerate much higher magnet fringe fields than do conventional photomultiplier tubes. Tests of the counters suggested a timing resolution[19] of 600 ps, which gives an effective resolution of 750 ps when a spread of 3% in the muon momentum is taken into account. (This spread produces a non-negligible dephasing of the ensemble muon polarization due to differences in time of flight through the magnet's fringe fields.) The extremely high fields of the experimental magnet interact with the muon beam line's focusing magnets to produce a spatially oscillating muon beam profile with an estimated maximum diameter of 18 mm — more than twice that of the sample.[20] For a fixed sample position, this makes the ratio of the number muons stopping in the sample (the superconducting signal) to those stopping in the cryostat (the background signal) vary with the applied field.

VI. DATA ANALYSIS

When fitting the data, one might hope to obtain the theoretical line shape in the London "medium field" limit by simply scaling a single representative line shape by λ^{-2}; however, since the field cutoff at the vortex core is evident in the high field data (and is an important aspect of the measurement), this was not possible and it was necessary to recalculate the line shape directly for every significant change of the fitted parameters. The spatial distribution of the local magnetic field $B(\mathbf{r})$ was calculated for given values λ^{-2}, H_{c2}, and B_0 over an array of positions within the FLL unit cell and then interpolated to increase the effective number of points. From this, a probability distribution of local fields $n(B)$ was calculated. Then $n(B)$ was convoluted with a Gaussian of width σ_B [Eq. (4.1)] to represent the effects of nuclear dipolar fields, disorder in the FLL, and the Gaussian apodization[9] used in the Fourier transform of the data. Since the time signal is completely depolarized within about 2 μs, except for the slowly relaxing background signal, apodization reduces the noise in the Fourier transform without much distortion of the results. Apodization does introduce an additional width in the experimental Fourier transform, but it is smaller than either the intrinsic width of the ideal line shape or the corrected convolution. Finally, this "smeared" theoretical line shape was multiplied by an overall normalization. In addition, a simple Gaussian line with width δ_b, average field B_b, and normalization n_b was added to fit the background signal due to muons stopping in the sample mounting or the cryostat rather than in the sample.

For a given line shape $n(B)$ corresponding to a spatial field distribution $B(\mathbf{r}; B_0, \lambda^{-2}, H_{c2})$, there is a large range of values for the penetration depth and coherence length which produce nearly the same line shape.[21] Therefore it would be advantageous to use reliable values for $\xi(T)$ or $H_{c2}(T)$ from the literature, and thereby determine $\lambda(T)$ to great accuracy, because the line shape is less sensitive to $\xi(T)$—the extreme case being low temperatures where the conditions approach the London

"medium field" limit ($B_0 \ll H_{c2}$) and the line shape is nearly independent of ξ. Unfortunately, as discussed earlier, reliable values for $H_{c2}(T)$ in $YBa_2Cu_3O_{6.95}$ are not available over the whole temperature range because $H_{c2}(T)$ is very high and therefore difficult to measure. However, the ambiguity can be reduced[21] by simultaneously fitting several runs at the same temperature and different applied fields with shared parameters λ^{-2} and H_{c2}.

As an example of this "global" fitting technique, Fig. 6 shows the χ^2 fit quality factor χ^2_B over a grid of fixed values of λ^{-2} and H_{c2} for individual runs at 70 K in fields of 1.9 T, 4.1 T, 4.7 T, and 6.5 T as well as $\chi^2_T \equiv \sum_B \chi^2_B$ for the four runs fitted simultaneously. The best (lowest) χ^2_B for each run is highlighted by a solid square and increasing values of χ^2_B are indicated by smaller and smaller boxes, thereby roughly indicating χ^2_B contours in λ^{-2}, H_{c2} space of similar fit quality. If λ^{-2} and H_{c2} were completely independent variables, one would expect elliptical contours near the minimum. Instead we see curved "troughs," which suggest a high degree of correlation. These troughs tend to follow the contours of constant average field B_0 extracted from the fits with the lowest χ^2_B in the individual runs (marked R in the figures) and the lowest total χ^2_T in the combined result (marked T). This suggests that along the contour, the line shapes are nearly identical. Because the individual χ^2_B contours for different fields have different slopes, the total χ^2_T contours tend to have deeper and less troughlike minima. In other words, by fitting to a common λ^{-2} and a common H_{c2} for runs of different fields at a given temperature, both λ^{-2} and H_{c2} can be determined from the μSR line shapes. The uncertainties in the best values of λ^{-2} and H_{c2} were estimated in terms of the distance from the best-fit point $\chi^2_{T,\min}$ to the locus of $\chi^2_{T,\min} + 1$ (highlighted by solid diamonds). If there were no points within 2 of $\chi^2_{T,\min}$,

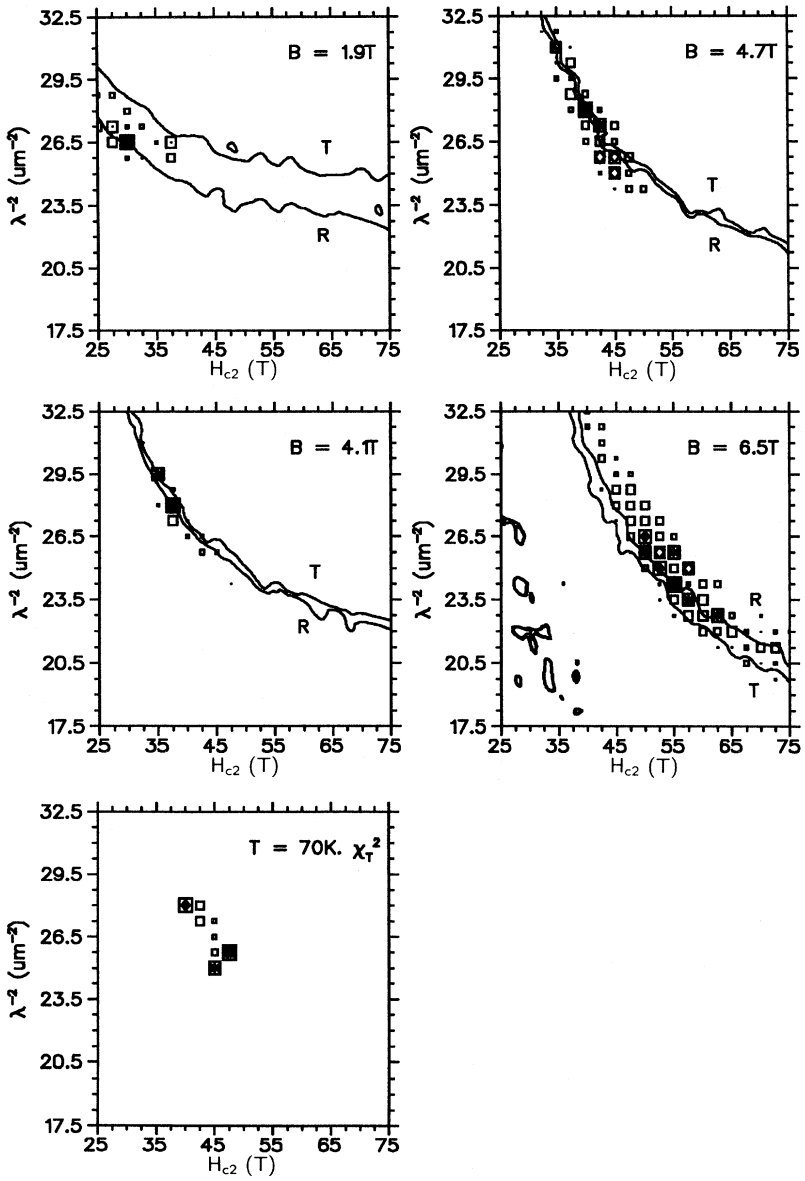

FIG. 6. Fit quality factor χ^2_B as a function of λ^{-2} and H_{c2} for individual runs at $T = 70$ K in fields of 1.9 T, 4.1 T, 4.7 T, and 6.5 T (left and center) and the total χ^2 ($\chi^2_T = \sum_B \chi^2_B$) resulting from simultaneous ("global") fits (right). The solid square marks the minimum (χ^2_m), open squares with solid diamonds mark $\chi^2 \leq \chi^2_m + 1$, open squares with stars mark $\chi^2 \leq \chi^2_m + 2$, and open squares with open diamonds mark $\chi^2 \leq \chi^2_m + 3$. The smaller boxes represent higher values of χ^2 up to $\chi^2_m + 10$. The curve marked R is a contour of those fits which have the same average field (B_0) as the best fit for the run. (Relative to the background field, $B_0 - B_b = -4.07$ G for $B_b = 1.9$ T, $B_0 - B_b = -5.34$ G for $B_b = 4.1$ T, $B_0 - B_b = -4.91$ G for $B_b = 4.7$ T, and $B_0 - B_b = -9.97$ G for $B_b = 6.5$ T for curves R.) The curve marked T is the contour of those fits which have the same average field (B_0) as the best global fit for the 70 K runs. ($B_0 - B_b = -2.57$ G for $B_b = 1.9$ T, $B_0 - B_b = -5.09$ G for $B_b = 4.1$ T, $B_0 - B_b = -4.72$ G for $B_b = 4.7$ T, and $B_0 - B_b = -10.47$ G for $B_b = 6.5$ T for curves T.)

then the uncertainties were estimated to be the step size in the grid of λ^{-2} and H_{c2} over which χ^2_T was evaluated. Due to the relatively coarse step size, the error estimates for λ^{-2} and H_{c2} are sometimes rather rough.

VII. RESULTS

A. Line shapes

Figures 7, 8, 9, and 10 show the experimental line shapes and fits for all measured fields at selected temperatures. The line shapes are all shown relative to the background signal (centered at 0 G) and have an arbitrary vertical offset. Because the μSR signal amplitude is reduced with increasing applied field due to loss of timing resolution and muon dephasing, the Fourier amplitudes have been renormalized so that the superconducting line shapes all have the same area. These figures demonstrate that, with increasing applied field, the line shape narrows slightly and that the difference between the field at the vortex core and the average field is reduced, as predicted by the presence of ξ in Eq. (3.4). These changes in the line shape are most dramatic at 70 K (Fig. 10) where the applied fields (1.9 T, 4.1 T, 4.7 T, and 6.5 T) cover a large range of reduced fields ($b = 0.04$, 0.09, 0.10, and 0.14, respectively). In the highest measured field (6.5 T), the line shape has a very distinct high field cutoff, while at the lowest field (1.9 T) it looks almost London like with the cutoff field nearly lost in the noise.

Figures 1–4 in Ref. 22 show the experimental line shapes and fits for all measured temperatures at each applied field. The linewidth increases with decreasing temperature, reflecting the temperature dependence of λ.

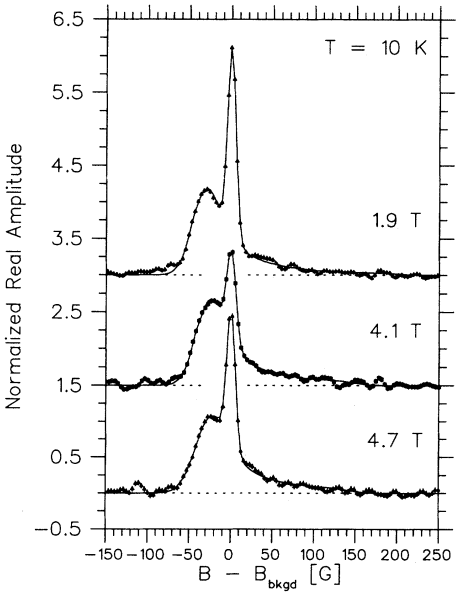

FIG. 7. High field μSR line shapes and fits to the modified London model at $T = 10$ K.

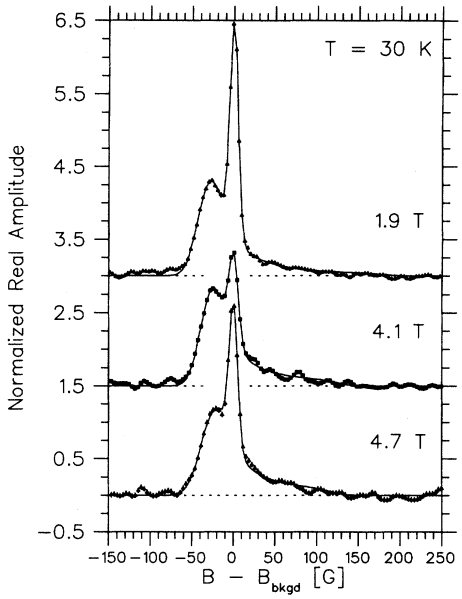

FIG. 8. High field μSR line shapes and fits to the modified London model at $T = 30$ K.

B. Penetration depth, upper critical field, and Ginzburg-Landau parameter

Figure 11 shows the temperature dependence of the best-fit values of λ_{ab}^{-2}, the inverse square of the penetration depth in the copper oxide planes. At 10 K, the value of the magnetic penetration depth is $\lambda_{ab}(10\,\mathrm{K}) = 0.149 \pm 0.002\,\mu$m. Fitting to a power law

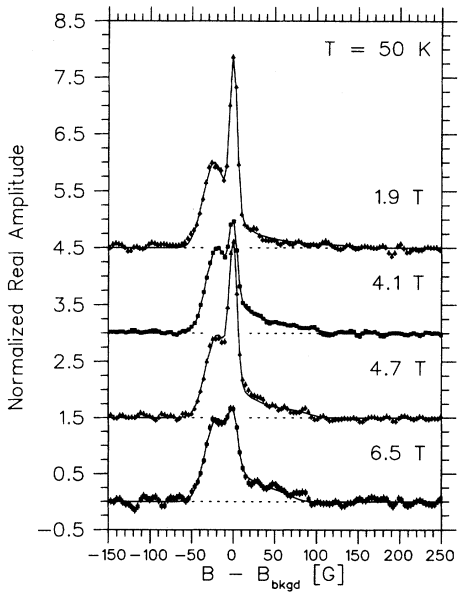

FIG. 9. High field μSR line shapes and fits to the modified London model at $T = 50$ K.

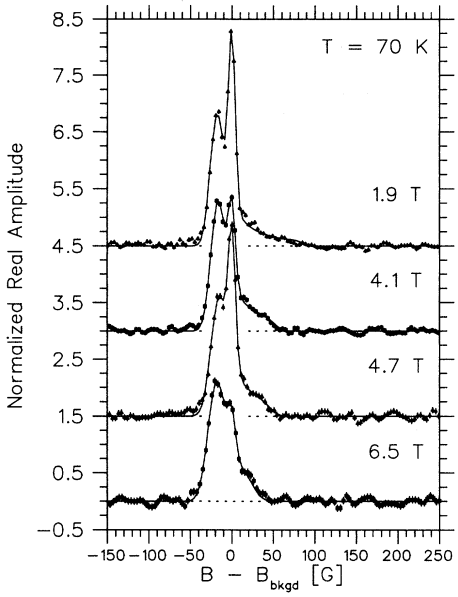

FIG. 10. High field μSR line shapes and fits to the modified London model at $T = 70$ K.

$$\lambda^{-2} \propto 1 - \{T/T_c\}^p \tag{7.1}$$

yields an exponent of $p = 2.89 \pm 0.23$, which does not support the Gorter-Casimir version of the two-fluid temperature dependence with $p = 4$ reported in sintered powder samples.[23,24] Gorter-Casimir behavior is usually interpreted as being indicative of strong-coupling s-wave superconductivity. The BCS weak-coupling s-wave temperature dependence does not fit as well as the power law.

Figure 12 shows the temperature dependence of the upper critical field H_{c2} (which we assume is proportional to ξ^{-2}) when $\mathbf{B}_0 \| \hat{\mathbf{c}}$. The value of $H_{c2}(10\,\mathrm{K}) = 90 \pm 10$ T corresponds to a coherence length in the planes of $\xi_{ab}(10\,\mathrm{K}) = 1.9 \pm 0.1$ nm. Since at lower temperatures the vortex core size is small and therefore has relatively little influence on the line shape, results below 30 K are not so well determined, and were therefore excluded from the fits to the various models. (The 20 K runs also have

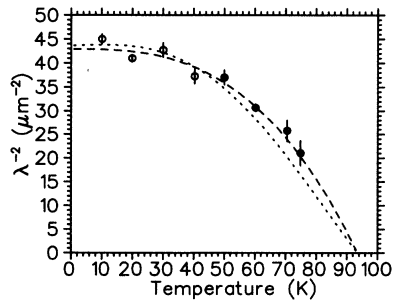

FIG. 11. $\lambda_{ab}^{-2}(T)$ from global fits of the high field data. The dashed line is a fit to $\lambda_{ab}^{-2}(T) = c(1 - \{T/T_c\}^p)$ (see Table I). The dotted line is a fit to BCS s-wave theory, with $\lambda_{ab}^{-2}(0) = 43.6 \pm 1.0\,\mu\mathrm{m}^{-2}$.

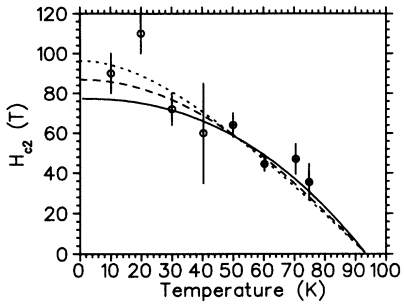

FIG. 12. The upper critical field $H_{c2}(T) = \phi_0/(2\pi\xi^2)$ for $\mathbf{B}_0 \| \hat{\mathbf{c}}$ from global fits of the high field data. The low-temperature runs at 10 K and 20 K were excluded from the fits. The solid line is a fit to $H_{c2}(T) = c(1 - \{T/T_c\}^p)$ (see Table I). The dotted line is a fit to the temperature dependence of H_{c2} for an s-wave BCS weak-coupling isotropic superconductor, with $dH_{c2}/dT\,|_{T=T_c} = -1.429 \pm 0.083$ T/K. The dashed line is a fit to the temperature dependence of H_{c2} for a superconductor with a cylindrical Fermi surface (i.e., 2D), with $dH_{c2}/dT\,|_{T=T_c} = -1.511 \pm 0.078$ T/K.

significantly fewer events than the 10 K and 30 K runs, and so the 20 K results are even less reliable.) In Fig. 12, the weak-coupling s-wave BCS temperature dependence for H_{c2} in an isotropic superconductor cannot be distinguished from that in a 2D superconductor with a cylindrical Fermi surface.[1] Fitting to a power law yields an exponent close to 2 (see Table I). All other techniques[4–8] also find it difficult to reliably measure the low-temperature values of $H_{c2}(T) \propto \xi^{-2}(T)$ which are critical for determining which theory best describes $H_{c2}(T)$.

The Ginzburg-Landau parameter $\kappa_{ab} = \lambda_{ab}/\xi_{ab}$ (see Fig. 13) shows essentially no temperature dependence if one ignores the points below 30 K where the values of H_{c2} are less reliable. The fit to a constant Ginzburg-Landau parameter gives $\kappa = 69.6 \pm 1.4$; κ should be independent of temperature if $YBa_2Cu_3O_{6.95}$ were a weak-coupling s-wave BCS superconductor. However, κ could have a weak temperature dependence (due to, for in-

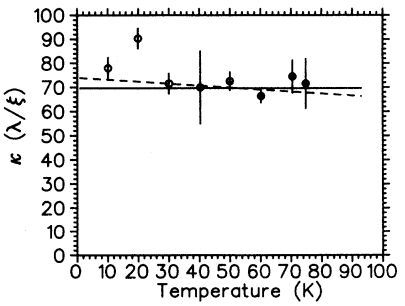

FIG. 13. The Ginzburg-Landau parameter κ from global fits of high field data. The solid line is a fit over the range 30 K to 75 K for a constant κ, with $\kappa = 69.6 \pm 1.4$. The dashed line is a fit to a linear temperature dependence, with $\kappa(0) = 74.0 \pm 6.0$ and a slope of $s = -0.08 \pm 0.11\,\mathrm{K}^{-1}$. Since H_{c2} has relatively little influence on the line shape at lower temperature, results below 30 K are not well determined, and so were excluded from the fits to the various models.

stance, strong coupling[25]) which is unnoticeable beneath the large error bars for the measured values $\kappa(T)$. Linear regression produces a line with a slope smaller than its own uncertainty, and so a linear fit is no better than a fit to a constant. However, the linear fit gives a more generous error of 6.0 for the value of κ at $T = 0$. Our value of κ is consistent with the average value of 72 found by Gohng and Finnemore[8] using reversible magnetization in the narrow temperature range between T_c and the irreversibility temperature.

Our data represent a relatively coarse sampling of temperatures, whereas a detailed investigation of $\lambda(T)$ in the low-temperature regime is necessary for distinguishing between possible pairing states — an s-wave superconductor should have an exponentially weak temperature behavior while a d-wave superconductor should have a linear T dependence. Two effects make interpreting intermediate temperatures rather difficult. First, the degree of strong coupling and the degree of gap anisotropy typically affect the behavior between $\frac{1}{4}T_c$ and $\frac{3}{4}T_c$. Second, impurity scattering makes both s-wave and d-wave models tend towards a T^{-2} dependence.[26,27] More extensive μ^+SR (Ref. 28) and microwave[29] measurements in similar $YBa_2Cu_3O_{6.95}$ crystals at lower field reveal a linear behavior in $\lambda(T<40\,\mathrm{K})$ suggestive of d-wave superconductivity, which confirms our tentative conclusion that $\lambda(T)$ seems to be inconsistent with an s-wave pairing state. It is perplexing that high quality single crystals show a temperature dependence significantly different from that of unoriented sintered powders. The sintered powders may have more atomic impurity sites and/or structural defects which serve as scattering sites; small grain sizes may also increase the effect of inhomogeneous bulk flux expulsion.

Recent μ^+SR measurements on similar crystals[28] in fields of 0.5 T and 1.5 T concentrated on the temperature region below 40 K, employing the same model used here but assuming a constant $\kappa = 68$ and that $\sigma_B \propto \lambda^{-2}$ (see Sec. VII D) based on the present results. The observed "linearity" of the temperature dependence of $\lambda_{ab}(T < 30\,\mathrm{K})$ *decreases* with increasing fields. Above 30 K, the magnetic penetration depth appears to be independent of applied field. This suggests that our increased difficulty in fitting our data below 30 K may in part represent a breakdown of the model used, as well as the reduced effect of ξ upon the line shape. Moreover, since the data presented here are taken in fields larger than the 0.5 T and 1.5 T fields used by Sonier *et al.*,[28] the linear low-temperature behavior in $\lambda(T)$ may be largely quenched at our higher fields. This suggests restricting conclusions about $\kappa(T)$ to the temperature range 30–75 K, where no field dependence has been detected.

C. Local fields versus temperature

Figure 14 shows the temperature and field dependence of the maximum (B_V), cusp (B_C), and minimum (B_M) fields, relative to the average field B_0 of the superconducting signal. These fields are not the parameters used in the calculation of the line shape, but are features of the *unsmeared* theoretical line shape which, when convoluted with a Gaussian, fits the experimental data best when $\lambda^{-2}(T)$ and $H_{c2}(T)$ are shared for all fields at a given temperature T. The curves shown are the result of fits to $\{B_M, B_C, \text{or } B_V\} = c\,(1 - [T/T_c]^p)$, individual cases of which are listed in Table I. In all cases, the fitted exponent p is reduced when the applied field is increased, with the strongest effect for B_V. The reduction is due to the term $(1 - b)$ in Eq. (3.4) which represents the field dependence of the superconducting order parameter. Note that B_C and B_M have exponents p close to 2, while B_V has $1.0 < p < 1.5$ — all of which are smaller than that for λ^{-2}, which has p close to 3. For instance, if one were to fit the 4.1 T data with a Gaussian for the

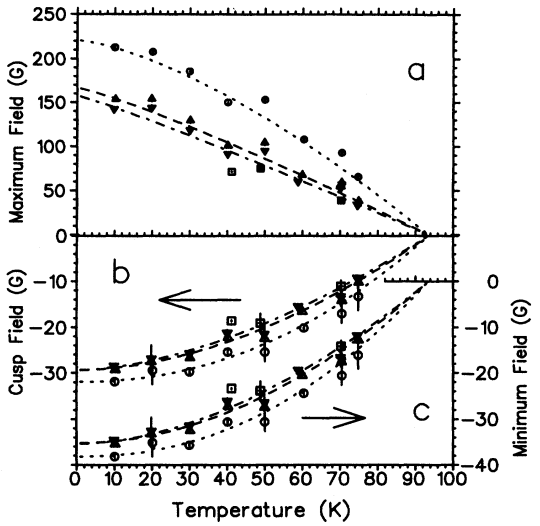

FIG. 14. Maximum (a), cusp (b), and minimum (c) fields relative to the average field in the superconductor, from global fits for applied fields of 1.9 T (circles, dotted curve), 4.1 T (triangles, dashed curve), 4.7 T (upside-down triangles, dotted-dashed curve), and 6.5 T (squares, without curve). See Table I for the parameters used in the curves. Errors for the maximum fields are underestimated.

TABLE I. Values of p and c for fits using $c\,(1 - \{T/T_c\}^p)$ in Figs. 11, 12, 14, and 15, with T_c fixed to 93.5 K.

	Power p	Constant c	
$\lambda_{ab}(T)$	2.89 ± 0.23	42.90 ± 0.88	(μm^{-2})
$H_{c2}(T)$	2.28 ± 0.76	77.0 ± 13.	(T)
$\sigma_B(T)$, $B = 1.9$ T	1.84 ± 0.13	13.66 ± 0.37	(G)
$\sigma_B(T)$, $B = 4.7$ T	1.96 ± 0.15	15.68 ± 0.44	(G)
B_M, $B = 1.9$ T	2.20 ± 0.13	−38.18 ± 0.66	(G)
B_M, $B = 4.1$ T	1.97 ± 0.12	−35.22 ± 0.90	(G)
B_M, $B = 4.7$ T	1.812 ± 0.055	−35.39 ± 0.46	(G)
B_C, $B = 1.9$ T	2.16 ± 0.13	−31.91 ± 0.55	(G)
B_C, $B = 4.1$ T	1.85 ± 0.10	−29.35 ± 0.71	(G)
B_C, $B = 4.7$ T	1.693 ± 0.056	−29.39 ± 0.42	(G)
B_V, $B = 1.9$ T	1.471 ± 0.078	220.6 ± 4.1	(G)
B_V, $B = 4.1$ T	1.163 ± 0.066	166.9 ± 4.9	(G)
B_V, $B = 4.7$ T	1.100 ± 0.076	157.6 ± 5.2	(G)

smeared cusp region, one would find a temperature dependence of the Gaussian's width of $p \approx 1.85$–2.0. This highlights the need for care when interpreting the temperature dependence of data taken in lower fields over a wide temperature range ($0 < T \leq T_c$) as being in the London "medium field" limit [$\lambda > L$ and $\xi \ll L$ and Eq. (3.3) is valid], which predicts that gross features of the line shape (such as the overall rms linewidth) will be proportional to λ^{-2}. In particular, data taken near T_c will have a higher reduced field b due to the temperature dependence of H_{c2} and will *not* be in the London "medium field" limit since ξ/L is no longer negligible.

The Meissner effect is not well determined by the μ^+SR data. At 70–75 K, the average internal field in the superconductor relative to the applied field (as determined by runs taken above T_c) is about -1 G at 1.9 T, -2 G at 4.1 T, -3 G at 4.7 T, and -2 G at 6.5 T. Since 70 K is below the irreversibility temperature and the FLL is locked in, further flux expulsion is prevented by pinning of the vortices. However, as the temperature decreases, the average field in the superconductor *increases* approximately linearly with temperature, which is not consistent with flux expulsion or creep. The fitted value of the average field is strongly influenced by the maximum field at the vortex core, which is more poorly determined at lower temperatures where the line shape has a very long, low amplitude, high field tail which is hard to fit accurately. Another possibility is that an admixture of a square FLL with the triangular lattice will deemphasize the tail relative to the cusp region of the line shape,[30] with the result that fits to a pure triangular lattice will overestimate the average field. A local preference for a square lattice at twin boundaries is likely.[31] It is plausible that in a d-wave superconductor[32] the vortex core might be somewhat rosette shaped, rather than circular, and therefore be a source of difficulty when fitting data with s-wave line shapes.

D. Disorder in the FLL

As explained earlier, the experimental line shapes show appreciable "smearing" relative to the theoretical line shapes; to mimic the effects of (1) nuclear dipolar fields, (2) apodization preceding the Fourier transform, and (3) the inherent disorder in the FLL, the theoretical line shapes were convoluted with a Gaussian. Figure 15 shows the convolution width (σ_B) after correcting (in quadrature) for the linewidth above T_c (due to nuclear dipolar fields and a distribution of Knight shifts) and for the Gaussian apodization used in the Fourier transform ($\sigma_{\rm apod}^{-1} = 2.5\,\mu$s for $T \leq 40$ K, corresponding to a width in the Fourier transform of 4.7 G, and $\sigma_{\rm apod}^{-1} = 3.0\,\mu$s for $50 \geq T \geq 75$ K, corresponding to a width of 3.9 G). The corrected convolution has a power-law temperature dependence with an exponent of about 2 (see Table I), which is very similar to the behavior of the maximum and cusp fields shown in Fig. 14. This qualitatively supports the assumption in Ref. 28 that $\sigma_B \propto \lambda^{-2}$ in lower fields.

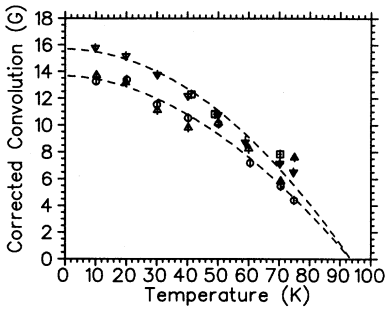

FIG. 15. The convolution width (σ_B) in gauss from global fits, after correction for the Gaussian apodization used in the Fourier transform and width of the nuclear dipolar field distribution as measured above T_c, for fields of 1.9 T (circles), 4.1 T (triangles), 4.7 T (upside-down triangles), and 6.5 T (squares). The dashed lines are fits to a power law (1.9 T top, 4.7 T bottom) (see Table I).

Figure 16 shows an estimate of $\langle s^2\rangle^{1/2}/L$, the square root of the mean square of the deviation of each vortex from its ideal position in the FLL as a fraction of the distance L between vortices, using σ_B, B_0, λ^{-2}, and H_{c2} in Eq. (4.3). The degree of disorder lies between about 5% and 6.5%, with the highest values occurring in the 4.7 T runs, all of which have a rather large background signal. Large backgrounds make fitting more difficult and lead to an artificially large convolution. In the narrowest line shapes (those at the higher temperatures and higher fields), the fits tend to misplace the cusp region because the cusp contains very few points in the discrete FFT. This also leads to an artificially large convolution. The results for 1.9 T, which show a slight reduction in $\langle s^2\rangle^{1/2}/L$ at larger temperatures, are more reliable than those for higher fields, which show a slight reduction followed by a larger increase at the highest temperatures. Other factors can contribute to the smearing, such as macroscopic field gradients due to the interaction of flux expulsion with pinning, different geometric factors due to the range of crystal sizes and shapes in the mosaic,

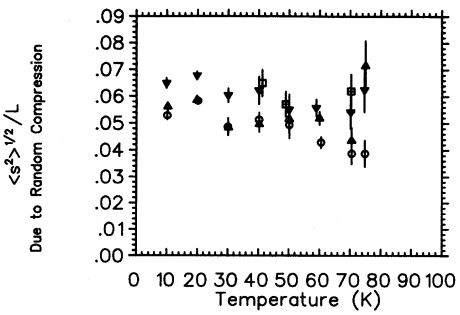

FIG. 16. Calculated values of $\langle s^2\rangle^{1/2}/L$, the square root of the mean square of the deviation of each vortex from its ideal position in the FLL normalized by the distance L between vortices, due to random compression for fields of 1.9 T (circles), 4.1 T (triangles), 4.7 T (upside-down triangles), and 6.5 T (squares).

and a spatial variation in the penetration depth. Because these factors probably affect the line shape in similar ways and therefore cannot easily be distinguished from the effects of local disorder in the FLL, these values of $\langle s^2\rangle^{1/2}/L$ should be taken as upper limits. In summary, $\langle s^2\rangle^{1/2}/L \leq 5.5\%$ and is nearly constant below 60 K, while above 60 K there may be a small decrease with increasing temperature. The vortices are definitely *not* in a glassy state (for which severe pinning would have totally destroyed the FLL), since the rms value of the disorder would be at least ≈ 10–$15\,\%$ in that case.

Results of ^{89}Y NMR experiments[33] in aligned $YBa_2Cu_3O_7$ with a field of 8.2 T applied parallel to the $\hat{\mathbf{c}}$ axis revealed thermal diffusion of vortices at a rate $4\times10^{-10}\exp(-E_a/T)\,\mathrm{cm}^2/\mathrm{s}$, with an activation energy of $E_a = 500$ K; in that experiment it was assumed that the NMR linewidth (due to the distribution of local fields) was proportional to the magnetic penetration depth $\lambda^{-2} \propto 1 - \{T/T_c\}^p$, with an exponent of $p = 4$. If one assumes our value for the rms displacement of the vortices, $\langle s^2\rangle^{1/2}/L \approx 5.5\,\%$ (0.93 nm at 8.2 T), this gives an estimate of 1.5 s at 40 K and 3 ms at 80 K for the time scale over which the vortices oscillate about their equilibrium positions in the pinned FLL. This suggests that the fluctuations of the vortices seen by NMR are observed as quasistatic disorder in μSR experiments. The orders of magnitude of the estimated time scales are not strongly affected by the assumptions made in the NMR paper. In particular, if a power-law exponent of 2 is assumed (consistent with our observed temperature dependence of the μSR linewidth), the diffusion rate changes to $20\times10^{-10}\exp(-E_a/T)\,\mathrm{cm}^2/\mathrm{s}$ with $E_a = 550$ K, which gives diffusion times of 1 s at 40 K and 1 ms at 80 K.

VIII. CONCLUSIONS

We have measured the μ^+SR line shape in single crystal $YBa_2Cu_3O_{6.95}$ in very high fields ($\mathbf{B}_0 \parallel \hat{\mathbf{c}}$) and have observed the maximum field due to the vortex core for the first time in any high-temperature superconductor. By simultaneously fitting several runs taken in different applied fields at the same temperature, we have been able to determine both $\lambda_{ab}^{-2}(T)$ and $H_{c2}(T) \propto \xi_{ab}^{-2}(T)$. At 10 K, $\lambda_{ab} = 0.15 \pm 0.01\,\mu$m, $\xi_{ab} \approx 1.9$ nm, and $H_{c2} \approx 90$ T. The temperature dependence of the magnetic penetration depth is consistent with other data[28,29] on similar crystals which do not show BCS s-wave behavior and are more consistent with d-wave superconductivity.[34] Due to the more subtle influence of ξ on the line shape, the scatter in $H_{c2}(T) \propto \xi_{ab}^{-2}(T)$, especially at low temperatures, discourages any conclusions about its detailed temperature dependence; however, within uncertainties $\kappa \equiv \lambda/\xi$ appears to be temperature independent.

While magnetic decoration experiments[35] can directly observe the FLL and its disorder, they are restricted to very low fields, typically less than 200 G. The degree of "smearing" of the μSR line shape, relative to the theoretical line shape for a perfect FLL, allows one to estimate the degree of disorder in any field accessible to μSR (up to about 6.5 T). In $YBa_2Cu_3O_{6.95}$, we have determined that the rms deviation of the vortices from their ideal positions in the FLL is less than 5.5% of the intervortex spacing, with no discernible field dependence. The disorder is due either to pinning of individual vortices or to thermal fluctuations in the positions of the vortices on a time scale which is quasistatic relative to the muon lifetime of 2.2 μs.

This particularly exhaustive analysis of the μSR line shape in $YBa_2Cu_3O_{6.95}$ serves to buttress certain simplifying assumptions which will aid future studies. First, our analysis confirms that the amount of smearing is proportional to the linewidth for the ideal FLL [$\sigma_B(T) \propto B_C(T) - B_M(T)$], which is proportional to $\lambda^{-2}(T)$ in lower fields. A much simpler analysis in terms of the linewidth alone (e.g., conventional fits to simple Gaussian relaxation functions in the time domain) should therefore be expected to yield meaningful results for $\lambda^{-2}(T)/\lambda^{-2}(0)$ at low fields and temperatures where the vortex cores are negligible, as long as the sizes of the individual superconducting crystals are not too small and all are aligned with their $\hat{\mathbf{c}}$ axes along the field; of course, such analyses will yield only a crude qualitative estimate for the absolute value of $\lambda(0)$.

Second, the simplest yet perhaps the most important result from this high field experiment is that in $YBa_2Cu_3O_{6.95}$ the Ginzburg-Landau parameter $\kappa_{ab} \equiv \lambda_{ab}/\xi_{ab}$ is constant with a value of 69.6 ± 1.4 over a large range of temperatures below the irreversibility temperature, at least down to 30/K. (By contrast, magnetization measurements[7,8] of κ are restricted to the region between the irreversibility temperature and T_c, which is a narrow range in $YBa_2Cu_3O_{6.95}$.) This allows data to be taken at higher fields and temperatures than the simple London model ($\kappa \gg 1$ and $\xi \ll L$) normally allows and to be analyzed with the correct line shapes without an inordinate amount of difficulty. However, one should not assume that all samples have exactly the same absolute value for κ, since no studies have been made of its dependence upon oxygen doping. If we presume that $YBa_2Cu_3O_{6.95}$ is a weak-coupling s-wave superconductor, the constancy of κ serves as a consistency check for the way that the data was fit. But such a presumption must be wrong, since the temperature dependence of λ_{ab} seems to rule out s-wave superconductivity.[28] If we do not assume any particular pairing state, our results demand that any theory for the mechanism of superconductivity in $YBa_2Cu_3O_{6.95}$ must predict a constant (or very weakly varying) κ. Various combinations[34,26,27,36,37] of s-, d-, and p-wave pairing, impurity scattering, paramagnetic contributions, and the degree of strong coupling can produce a vast array of behavior in $\lambda(T)$, $H_{c2}(T)$, $\xi(T)$, and $\kappa(T)$, much of which has not yet been calculated.

ACKNOWLEDGMENTS

This work was supported by the Natural Sciences and Engineering Research Council of Canada, by the Canadian Institute for Advanced Research, and, through TRIUMF, by the National Research Council of Canada. We gratefully acknowledge the beam line calculations of V. Aseev, J. Beveridge, and Jaap Doornbos and the technical assistance of K. Hoyle and C. Ballard.

* Present address: Dept. of Physics, Indiana University, Bloomington, IN 47405.
† Present address: Clarendon Lab., Oxford University, Oxford, U.K., OX1 3PU.
‡ Present address: Université Paris-Sud, Orsay, France.
§ Present address: Siemens Austria, PSE, 1100 Vienna, Austria.
** Present address: Physik-Institut, Universität Zürich, Zürich, Switzerland.

[1] J. Rammer, Physica C **177**, 421 (1991).
[2] E.H. Brandt, J. Low Temp. Phys. **73**, 355 (1988).
[3] J.R. Clem, in *Low Temperature Physics — LT14*, edited by M. Krusius and M. Vurio (North-Holland, Amsterdam, 1975), Vol. 2, p. 285.
[4] K. Nakao *et al.*, Phys. Rev. Lett. **63**, 97 (1989).
[5] F. Mueller *et al.*, Phyisca B **172**, 253 (1991).
[6] J. Goettee *et al.*, Physica B **194-196**, 1805 (1994).
[7] Z. Hao *et al.*, Phys. Rev. B **43**, 2844 (1991).
[8] J. Gohng and D. Finnemore, Phys. Rev. B **46**, 398 (1992).
[9] D.G. Fleming, J.H. Brewer, and P.W. Percival, in *Fourier, Haddemard and Hilbert Transforms in Chemistry*, edited by A.G. Marshall (Plenum, New York, 1982).
[10] A. Abrikosov, Sov. Phys. JETP **5**, 1174 (1957).
[11] W.H. Kleiner, L.M. Roth, and S.H. Aulter, Phys. Rev. **113**, A1226 (1964).
[12] E.H. Brandt, Phys. Rev. B **37**, 2349 (1988).
[13] E.H. Brandt, J. Low Temp. Phys. **26**, 709 (1977).
[14] A. Sidorenko, V. Smilga, and V. Fesenko, Hyperfine Interact. **63**, 49 (1990).
[15] R. Parks, *Superconductivity* (Marcel Dekker, New York, 1969), p. 860.
[16] D. Herlach *et al.*, Hyperfine Interact. **63**, 41 (1990).
[17] R. Liang *et al.*, Physica C **195**, 51 (1992).
[18] J.H. Brewer, Hyperfine Interact. **8**, 831 (1981).
[19] E. Holzschuh, Phys. Rev. B **27**, 102 (1983).
[20] V. Aseev and J. Beveridge, Design Note TRI-DN-92-1, TRIUMF, 4004 Wesbrook Mall, Vancouver, B.C., Canada, V6T 2A3 (unpublished).
[21] T.M. Riseman and J.H. Brewer, Hyperfine Interact. **87**, 597 (1994).
[22] T.M. Riseman *et al.*, Hyperfine Interact. **87**, 481 (1994).
[23] R.F. Kiefl *et al.*, Physica C **153-155**, 757 (1988).
[24] Y.J. Uemura *et al.*, Phys. Rev. B **38**, R909 (1988).
[25] R. Parks, *Superconductivity* (Marcel Dekker, New York, 1969).
[26] J. Annett, N. Goldenfeld, and S. Renn, Phys. Rev. B **43**, 2778 (1991).
[27] J.F. Annett, N. Goldenfeld, and S. Renn, in *Physical Properties of High Temperature Superconductors II*, edited by D. M. Ginsberg (World Scientific, Singapore, 1991), p. 571.
[28] J.E. Sonier *et al.*, Phys. Rev. Lett. **72**, 744 (1994).
[29] W.N. Hardy *et al.*, Phys. Rev. Lett. **70**, 3999 (1993).
[30] W. Fite and A.G. Redfield, Phys. Rev. Lett. **17**, 381 (1966).
[31] M. Yethiraj *et al.*, Phys. Rev. Lett. **70**, 857 (1993).
[32] S. Yip and J. Sauls, Phys. Rev. Lett. **69**, 2264 (1992).
[33] B. Suh, D. Torgeson, and F. Borsa, Phys. Rev. Lett. **71**, 3011 (1993).
[34] N. Bulut and D. Scalapino, Phys. Rev. B **45**, 2371 (1992).
[35] D. Bishop, P. Gammel, D. Huse, and C. Murray, Science **255**, 165 (1992) and references therein.
[36] M. Prohammer and J. Carbotte, Phys. Rev. B **43**, 5370 (1991).
[37] M. Prohammer and J. Carbotte, Phys. Rev. B **42**, 2032 (1990).